High-Affinity Adaptors for Switchable Recognition of Histidine-Tagged Proteins

Suman Lata,[†] Annett Reichel,[†] Roland Brock,[‡] Robert Tampé,[†] and Jacob Piehler*,[†]

Contribution from the Institute of Biochemistry, Johann Wolfgang Goethe-University, Frankfurt/Main, Germany, and Institute for Cell Biology, Eberhard Karls-University, Tübingen, Germany

Received February 2, 2005; E-mail: j.piehler@em.uni-frankfurt.de

Abstract: We aspired to create chemical recognition units, which bind oligohistidine tags with high affinity and stability, as tools for selectively attaching spectroscopic probes and other functional elements to recombinant proteins. Several supramolecular entities containing 2−4 nitrilotriacetic acid (NTA) moieties were synthesized, which additionally contained an amino group, to which fluorescein was coupled as a sensitive reporter probe. These multivalent chelator heads (MCH) (termed bis-, tris-, and tetrakis-NTA) were characterized with respect to their interaction with hexahistidine (H6)- and decahistidine (H10)-tagged targets. Substantially increased binding stability with increasing number of NTA moieties was observed by analytical size exclusion chromatography. The binding enthalpies as determined by isothermal titration calorimetry increased nearly additively with the number of possible coordinative bonds between chelator heads and tags. Yet, a substantial excess of histidines in the oligohistidine tag was required for obtaining fully additive binding enthalpies. Dissociation kinetics of MCH/oligohistidine complexes measured by fluorescence dequenching showed an increase in stability by 4 orders of magnitude compared to that of mono-NTA, and subnanomolar affinity was reached for tris-NTA. The gain in free energy with increasing multivalency was accompanied by an increasing loss of entropy, which was ascribed to the high flexibility of the binding partners. Numerous applications of these MCHs for noncovalent, high affinity, yet reversible tethering of spectroscopic probes and other functional elements to the recombinant proteins can be envisioned.

Introduction

In the current era of proteome research, generic tools for labeling, handling, modifying, and organizing proteins are increasingly demanded. During recent years, numerous methodologies for selective, site-specific conjugation of proteins with reporter molecules such as organic fluorophores,[1] spin labels,[2] nanoparticles,[3] or solid phases[4] have been reported. While several techniques for site-specific covalent coupling with a diverse range of functional elements are available,[5−7] noncovalent tethering through biological adaptor modules has most frequently served as an engineering principle for a selective and specific attachment to proteins.[8−14] The selectivity and specificity of labeling relies upon the recognition fidelity in these adaptors. Next to selectivity and site-specificity, ideal adaptors for noncovalent modification of proteins should also comply with the following requirements: (i) stoichiometrically defined and stable, yet reversible or even switchable binding with the protein under physiological conditions, (ii) site-specific and stoichiometric covalent coupling of the spectroscopic reporters or any other functional element by organic synthetic means, and (iii) small size for minimum effect on biochemical and physicochemical properties. Thus, ideal adaptors on one hand should be well compatible with organic synthesis yet soluble and stable under aqueous conditions.

Biological recognition units such as antibodies have reached high affinity and unmatched specificity toward their targets by an optimal interplay of many weak noncovalent forces such as hydrophobic interactions, hydrogen bonding, electrostatics, $\pi-\pi$ stacking, cation−π interaction, and so forth. However, proteins are large and chemically multifunctional macromolecules, which are incompatible with specific (organic) conjugation chemistry. Therefore, stoichiometrically and structurally well-defined attachment of spectroscopic probes is hardly possible. Furthermore, high-affinity binding of protein-based recognition units is often only reversible under drastic denaturing conditions

---

† Johann Wolfgang Goethe-University.
‡ Eberhard Karls-University.
 (1) Holmes, K. L.; Lantz, L. M. *Methods Cell Biol.* **2001**, *63*, 185−204.
 (2) Hubbell, W. L.; Gross, A.; Langen, R.; Lietzow, M. A. *Curr. Opin. Struct. Biol.* **1998**, *8*, 649−656.
 (3) Salata, O. *J. Nanobiotechnol.* **2004**, *2*, 3.
 (4) Cooper, M. A. *Anal. Bioanal. Chem.* **2003**, *377*, 834−842.
 (5) Yin, J.; Liu, F.; Li, X.; Walsh, C. T. *J. Am. Chem. Soc.* **2004**, *126*, 7754−7755.
 (6) George, N.; Pick, H.; Vogel, H.; Johnsson, N.; Johnsson, K. *J. Am. Chem. Soc.* **2004**, *126*, 8896−8897.
 (7) Griffin, B. A.; Adams, S. R.; Tsien, R. Y. *Science* **1998**, *281*, 269−272.
 (8) Farinas, J.; Verkman, A. S. *J. Biol. Chem.* **1999**, *274*, 7603−7606.
 (9) Marks, K. M.; Braun, P. D.; Nolan, G. P. *Proc. Natl. Acad. Sci. U.S.A.* **2004**, *101*, 9982−9987.
(10) Wu, M. M.; Llopis, J.; Adams, S.; McCaffery, J. M.; Kulomaa, M. S.; Machen, T. E.; Moore, H. P.; Tsien, R. Y. *Chem. Biol.* **2000**, *7*, 197−209.
(11) Chen, I.; Ting, A. Y. *Curr. Opin. Biotechnol.* **2005**, *16*, 35−40.
(12) Chen, I.; Howarth, M.; Lin, W.; Ting, A. Y. *Nat. Methods* **2005**, *2*, 99−104.

(13) Miller, L. W.; Cornish, V. W. *Curr. Opin. Chem. Biol.* **2005**, *9*, 56−61.
(14) Miller, L. W.; Sable, J.; Goelet, P.; Sheetz, M. P.; Cornish, V. W. *Angew. Chem., Int. Ed.* **2004**, *43*, 1672−1675.

---

because several different types of weak forces have to be interfered with simultaneously. Fast switchability of protein interaction (e.g., in signal transduction) therefore relies on complex conformational changes, which typically involve enzymatic processes or binding of ligands or metal ions. Without induced conformational changes, the fastest rate at which the switching may occur is the inherent dissociation rate constant of a given interaction, thereby making the stable yet switchable binding elements paradoxical.

While designing chemical recognition elements with specificities comparable to their biological counterparts is currently beyond scientific capabilities, multivalent interactions have been successfully exploited for achieving high stabilities of supramolecular ligand/receptor complexes.[15−23] Another key advantage of multivalent interaction is the possibility to efficiently diminish its stability to that of the individual interaction by adding a monovalent competitor,[15] enabling for fast dissociating multivalent complexes under mild conditions. For designing multivalent chemical receptors for recognizing short peptide sequences, coordinative interaction is ideally suited: it is optimally tight compared to other weak interactions, independent of ionic strength, and relatively specific as only the typically rarely occurring amino acids histidine and cysteine exhibit substantial affinity toward transition metal ions. Transition metals chelated by nitrilotriacetic acid (NTA) or other chelators have been successfully applied for purification[24,25] and detection[25,26] of oligohistidine-tagged proteins, as well as for immobilization on surfaces[27−31] and for tethering to lipid membranes.[32−34] Fast dissociation of this interaction under mild conditions is readily achieved by adding competitors such as imidazole. Furthermore, the interaction may be switched by adding or removing the metal ion. While individual Me:NTA-oligohistidine complexes (which are typically formed by two coordination bonds) are of very low affinity ($K_D \approx 10\ \mu M$) and stability,[35−38] stable binding to surfaces densely covered with

NTA has been observed.[27,28,39,40] Apparently, stable interaction at interfaces is possible by multipoint attachment[40−42] (i.e., multivalent interaction) since the hexahistidine tag provides binding sites for three NTA moieties and larger oligohistidine tags even more. Indeed, cyanine dyes conjugated with two NTA moieties were shown to bind hexahistidine tags in solution with increased affinity.[36]

Here, we aimed to design high-affinity adaptors for oligohistidine-tagged proteins by incorporating multiple NTA moieties into single supramolecular entities, which can be site-specifically coupled with spectroscopic or biochemical probes using organic synthetic chemistry. We used dendritic and cyclic scaffolds for synthesizing such multivalent chelator headgroups (MCH) with two, three, and four NTA moieties. By conjugating these MCHs with a fluorescent dye, we incorporated a reporter, which was useful for concentration determination and for studying the kinetics of the interaction with hexa- and decahistidine tags. Furthermore, the thermodynamics of these interactions were assessed by isothermal titration calorimetry (ITC). The tremendous increase in complex stabilities achieved by these MCHs enabled stable and stoichiometric conjugation of proteins with affinities reaching subnanomolar levels.

Experimental Section

Synthesis of the MCH. The synthesis of the multivalent chelator heads is outlined in Scheme 1; the details are given in Supporting Information.

t-Butyl ester-protected NTA synthons (**3** and **12**) were derived from commercially available α-amino acid derivatives. The amino-functionalized synthon **3** was obtained from an appropriately protected L-lysine derivative as described earlier,[35] and the carboxy-functionalized synthon **12** was accordingly obtained from a protected L-glutamic acid. These synthons were then grafted onto structurally different scaffolds by amide bond formation. The other functional groups (amine and carboxyl group) while interfering were kept protected orthogonally to *tert*-butyl esters by conversion into benzyl carbamate and benzyl ester, respectively. Synthon **3** was doubled by coupling to the carboxyl groups of an L-glutamic acid scaffold (**4**), resulting in amino-functionalized **6** and the second-generation amino-functionalized **8**. Synthon **12** was grafted in triplicate onto a tetraaza cyclam (**9**) under stoichiometric control to yield **13**. The chelator head precursors (**3**, **6**, **8**, and **13**) were further modified to present a primary amine functionality followed by deprotection of the NTA heads (**16**, **17**, **18**, and **19**).

Adaptor/Reporter Conjugates. As a sensitive probe for monitoring interactions, fluorescein was coupled to the primary amino group of the MCH **16**, **17**, **18**, and **19** by using a carboxyfluorescein NHS ester (Fluka). The products were purified by preparative thin-layer chromatography and by anion exchange chromatography (HiTrap Q, Amersham Biosciences) in 20 mM HEPES, pH 7.0, and incubated with a stoichiometric excess of nickel chloride. For the removal of the excess nickel(II) ions, an additional step of anion exchange chromatography

(15) Rao, J.; Lahiri, J.; Isaacs, L.; Weis, R. M.; Whitesides, G. M. *Science* **1998**, *280*, 708−711.
(16) Kitov, P. I.; Sadowska, J. M.; Mulvey, G.; Armstrong, G. D.; Ling, H.; Pannu, N. S.; Read, R. J.; Bundle, D. R. *Nature* **2000**, *403*, 669−672.
(17) Lee, R. T.; Lee, Y. C. *Glycoconjugate J.* **2000**, *17*, 543−551.
(18) Mourez, M.; Kane, R. S.; Mogridge, J.; Metallo, S.; Deschatelets, P.; Sellman, B. R.; Whitesides, G. M.; Collier, R. J. *Nat. Biotechnol.* **2001**, *19*, 958−961.
(19) Lundquist, J. J.; Toone, E. J. *Chem. Rev.* **2002**, *102*, 555−578.
(20) Zhang, Z.; Merritt, E. A.; Ahn, M.; Roach, C.; Hou, Z.; Verlinde, C. L.; Hol, W. G.; Fan, E. *J. Am. Chem. Soc.* **2002**, *124*, 12991−12998.
(21) Christensen, T.; Gooden, D. M.; Kung, J. E.; Toone, E. J. *J. Am. Chem. Soc.* **2003**, *125*, 7357−7366.
(22) Mulder, A.; Auletta, T.; Sartori, A.; Del Ciotto, S.; Casnati, A.; Ungaro, R.; Huskens, J.; Reinhoudt, D. N. *J. Am. Chem. Soc.* **2004**, *126*, 6627−6636.
(23) Benito, J. M.; Gomez-Garcia, M.; Ortiz Mellet, C.; Baussanne, I.; Defaye, J.; Garcia Fernandez, J. M. *J. Am. Chem. Soc.* **2004**, *126*, 10355−10363.
(24) Hochuli, E.; Dobeli, H.; Schacher, A. *J. Chromatogr.* **1987**, *411*, 177−184.
(25) Ueda, E. K.; Gout, P. W.; Morganti, L. *J. Chromatogr., A* **2003**, *988*, 1−23.
(26) Hart, C.; Schulenberg, B.; Diwu, Z.; Leung, W. Y.; Patton, W. F. *Electrophoresis* **2003**, *24*, 599−610.
(27) Sigal, G. B.; Bamdad, C.; Barberis, A.; Strominger, J.; Whitesides, G. M. *Anal. Chem.* **1996**, *68*, 490−497.
(28) Gershon, P. D.; Khilko, S. *J. Immunol. Methods* **1995**, *183*, 65−76.
(29) Schmid, E. L.; Keller, T. A.; Dienes, Z.; Vogel, H. *Anal. Chem.* **1997**, *69*, 1979−1985.
(30) Xu, C.; Xu, K.; Gu, H.; Zhong, X.; Guo, Z.; Zheng, R.; Zhang, X.; Xu, B. *J. Am. Chem. Soc.* **2004**, *126*, 3392−3393.
(31) Schmitt, L.; Ludwig, M.; Gaub, H. E.; Tampe, R. *Biophys. J.* **2000**, *78*, 3275−3285.
(32) Schmitt, L.; Dietrich, C.; Tampe, R. *J. Am. Chem. Soc.* **1994**, *116*, 8485−8491.
(33) Dietrich, C.; Schmitt, L.; Tampe, R. *Proc. Natl. Acad. Sci. U.S.A.* **1995**, *92*, 9014−9018.
(34) Dorn, I. T.; Eschrich, R.; Seemuller, E.; Guckenberger, R.; Tampe, R. *J. Mol. Biol.* **1999**, *288*, 1027−1036.

(35) Dorn, I. T.; Neumaier, K. R.; Tampe, R. *J. Am. Chem. Soc.* **1998**, *120*, 2753−2763.
(36) Kapanidis, A. N.; Ebright, Y. W.; Ebright, R. H. *J. Am. Chem. Soc.* **2001**, *123*, 12123−12125.
(37) Hutschenreiter, S.; Neumann, L.; Radler, U.; Schmitt, L.; Tampe, R. *ChemBioChem* **2003**, *4*, 1340−1344.
(38) Guignet, E. G.; Hovius, R.; Vogel, H. *Nat. Biotechnol.* **2004**, *22*, 440−444.
(39) Nieba, L.; Nieba-Axmann, S. E.; Persson, A.; Hamalainen, M.; Edebratt, F.; Hansson, A.; Lidholm, J.; Magnusson, K.; Karlsson, A. F.; Pluckthun, A. *Anal. Biochem.* **1997**, *252*, 217−228.
(40) Dorn, I. T.; Pawlitschko, K.; Pettinger, S. C.; Tampe, R. *Biol. Chem.* **1998**, *379*, 1151−1159.
(41) Johnson, R. D.; Todd, R. J.; Arnold, F. H. *J. Chromatogr., A* **1996**, *725*, 225−235.
(42) Lata, S.; Piehler, J. *Anal. Chem.* **2005**, *77*, 1096−1105.

Scheme 1. Synthesis of the Chelator Building Blocks and the Multivalent Chelator Headgroups[a]
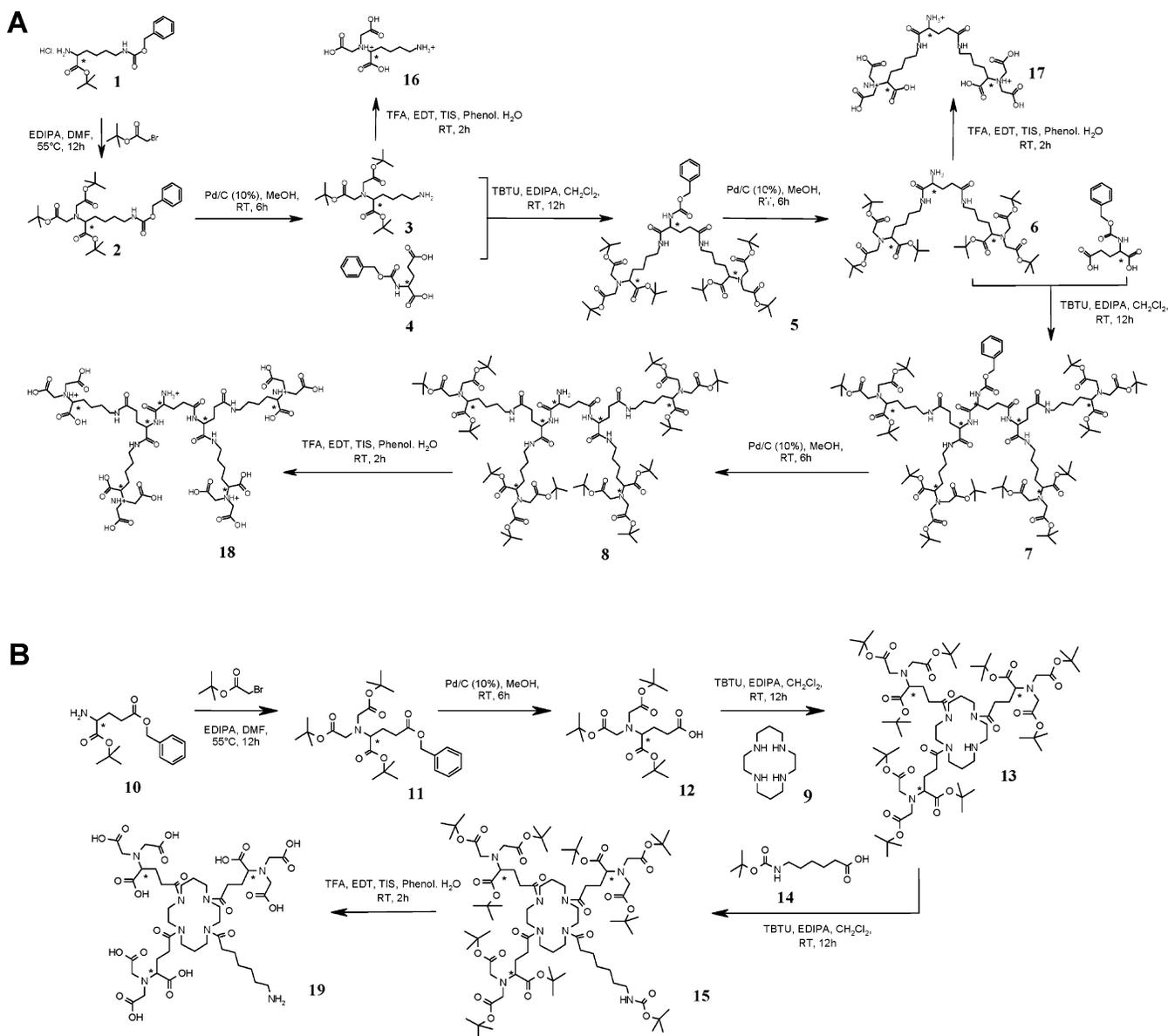
[a] (A) mono-NTA, as well as bis-NTA and tetrakis-NTA obtained by a dendrimer approach. (B) tris-NTA derived from a cyclic scaffold.

under the same conditions was carried out. The structures of the fluorescein-conjugated chelator heads after nickel(II) ion loading (**20**, **21**, **22**, and **23**), used in all the assays to follow, are shown in Figure 1.

Protein Expression and Purification. Wild-type extracellular domain of the human type I interferon receptor subunit ifnar2 (ifnar2-EC) variants with a C-terminal hexahistidine tag (ifnar2-H6) and a C-terminal decahistidine-tag (ifnar2-H10) were expressed and purified as reported earlier.[43] Maltose binding protein (MBP) with a C-terminal decahistidine and a hexahistidine tag (MBP-H10 and MBP-H6, respectively) were expressed and purified as previously described.[42] To check the integrity of the histidine tag, the purified proteins were analytically digested with factor Xa, and the molecular mass of the cleaved peptide was confirmed by MALDI-MS. All purified proteins were more than 95% homogeneous and monomeric as detected by nonreducing SDS-PAGE and size exclusion chromatography (SEC).

Analytical Size Exclusion Chromatography. Two-fold molar excess of the chelator heads (10 μM) was incubated with the

oligohistidine-tagged ifnar2-EC (5 μM) in 20 mM HEPES, pH 7.5, and 150 mM NaCl (HEPES-buffered saline, HBS) for 20 min. The sample was then loaded onto an SEC column (Superdex 200 PC 3.2/30) in a SMART system (Amersham Biosciences), and elution was monitored at 280 and 490 nm. To determine the relative amount of protein, the absorbance at 280 nm was corrected by subtracting the contribution of the fluorescence dye, which was determined from the absorbance at 490 nm. The chromatograms were normalized to the corrected absorption at 280 nm. Thus, the relative height of the 490-nm signal is a measure of labeling efficiency and hence complex stability. A 280 nm:490 nm ratio of ~1:2.5 was expected for a 1:1 complex.

Isothermal Titration Calorimetry. Calorimetric measurements were carried out using a VP-ITC instrument with a cell volume of 1.4115 mL (MicroCal, LLC). For ITC measurements, the proteins were purified in the same batch of the stock buffer as used for dilution of the sample and injectant. Exclusively one single batch of buffer was used for sample preparation and dilution for the chelator heads as well as the proteins. The background heat changes were negligible under these conditions. Interaction constants characterizing the chelator head

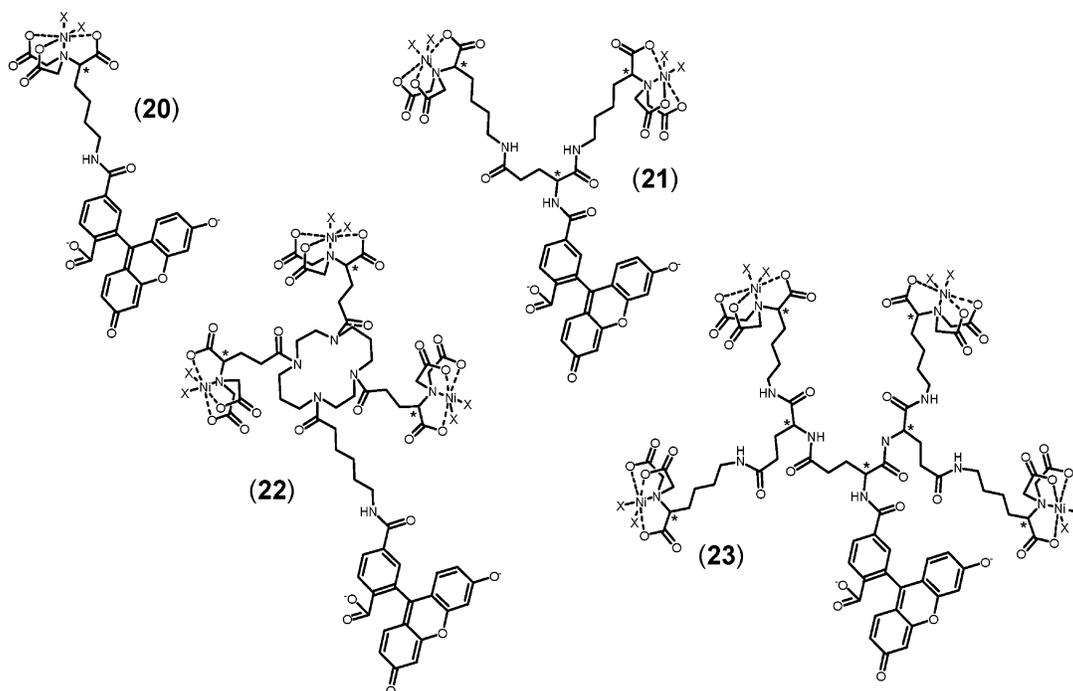(43) Piehler, J.; Schreiber, G. *J. Mol. Biol.* **1999**, *289*, 57−67.

Figure 1. Chemical structures of the carboxyfluorescein-conjugated chelator heads: mono-NTA-Fluo (**20**), bis-NTA-Fluo (**21**), tris-NTA-Fluo (**22**), and tetrakis-NTA-Fluo (**23**). The conjugates are shown loaded with nickel(II) ions as used for interaction studies in solution. The two remaining coordination sites of the NTA-complexed nickel(II) ions are occupied by general ligands X, and possible charges are therefore omitted.

oligohistidine tag interactions were determined by direct titration at pH 7.5 in HBS at 25 °C. The interaction assessments were carried out by adding the tagged protein or peptides to the chelator head solution in the cell. The solution in the cell was stirred at 800 rpm by the syringe to ensure rapid mixing. Typically 4–10 μL of the injectant was added over 30 s with an adequate interval between the injections to allow complete equilibration, and the heat change was monitored continuously upon addition of each injection of the titrant as a function of time. The data were analyzed using the Origin software package supplied by MicroCal. An interaction model assuming n independent and equivalent binding sites was applied, and the stoichiometry n, change in enthalpy $\Delta H°$, and binding constant K_D were iteratively fitted.

Time-Resolved Fluorescence Measurements. The kinetics of the chelator/oligohistidine tag complex formation and dissociation were measured using carboxyfluorescein-labeled H6 and H10 peptides. Upon complex formation of these peptides with the Ni^{2+}-loaded chelator/ carboxyfluorescein conjugates, strong fluorescence quenching was observed (Figure 2), which was probably mainly due to the chelated transition metal ions.[37,44,45] This effect was used as a readout for following the interaction in real time.

Association kinetics for all the chelator heads and the dissociation kinetics for mono-NTA were measured at 25 °C using an Applied Photophysics (π* 180 CDF) stopped flow spectrometer equipped with a photomultiplier tube and thermostat. The fluorophores were excited at 490 nm, and the signal was collected through a 515-nm long pass filter using a photomultiplier tube. The dissociation kinetics for the MCHs were measured with a fluorescence spectrometer (Varian Cary Eclipse) by exciting the fluorophores at 470 nm. Depending upon the kinetics of the process, single wavelength (510 nm) or spectral (490– 700 nm) data acquisition was carried out. Kinetics were fitted using Origin (Microcal Software) or Biaevaluation 2.1 (Biacore) for explicit models, and Berkeley Madonna (UCB) for numerical integration. For MCH/oligohistidine tag interactions, the dissociation kinetics were measured by chasing the fluorescein-labeled tag with nonlabeled MBP-
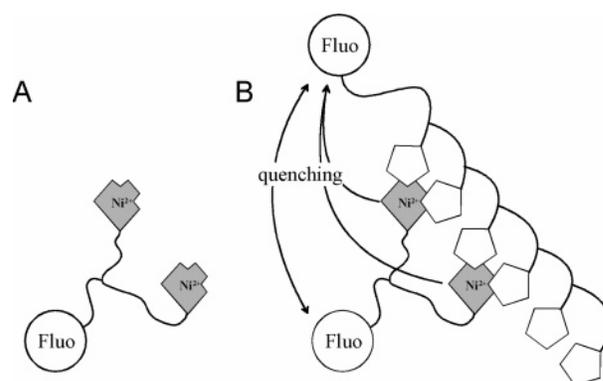
(44) Kemlo, J. A.; Shepherd, T. M. *Chem. Phys. Lett.* **1977**, *47*, 158–162.
(45) Fabbrizzi, L.; Licchelli, M.; Pallavicini, P.; Sacchi, D.; Taglietti, A. *Analyst* **1996**, *121*, 1763–1768.

Figure 2. Schematic representation of bis-NTA coupled to fluorescein (A) and its complex with fluorescein-labeled H6 (B). The quenching processes leading to fluorescence decay upon complex formation are indicated by the arrows.

H10. MBP-H10 (5 μM) was added to an equilibrated complex (500 nM each) of a given interaction pair in a cuvette, and the fluorescence at 520 nm was acquired as a function of time for up to 1 h. The equilibrium signal was determined after overnight incubation. For evaluation and comparison of the curves, the fluorescence signal at t_0 was subtracted and the curves were inverted and normalized to the equilibrium signal amplitude. The dissociation rate constant k_d was determined from these curves by fitting a first-order kinetics model:

$$S(t) = S_0 \cdot \exp[-k_d \cdot (t - t_0)] \qquad (1)$$

where $S(t)$ is the signal at time t, and S_0 is the equilibrium signal amplitude. The association kinetics for MCHs with oligohistidine were measured by mixing equal volumes of the chelator head (10 μM) and the oligohistidine tag (10 μM), leading to a final concentration of 5 μM of each. Since the association under these conditions was much faster than dissociation for all MCH/oligohistidine pairs, the curves

Table 1. Binding Parameters of the Chelator/Oligohistidine Complexes

	mono-NTA		bis-NTA		tris-NTA		tetrakis-NTA	
	H6	H10	H6	H10	H6	H10	H6	H10
m/r^a	2/4	2/8	4/2	4/6	6/0	6/4	6/2	8/2
$\Gamma\ ()^b$	$\sim$0	$\sim$0	$\sim$0.15	$\sim$1	$\sim$1	$\sim$1	$\sim$1	$\sim$1
$n\ ()^c$	0.35	−	1	1	1	1	1	1
K_D (nM)^d	$(14 \pm 4) \times 10^3$	−	270 ± 50	240 ± 50	20 ± 10	40 ± 20	40 ± 20	80 ± 30
$\Delta H°$ (kcal/mol)^e	-40.9 ± 1.5	−	-25.0 ± 1.0	-27.9 ± 1.1	-35.0 ± 1.2	-41.4 ± 1.5	-37.5 ± 1.3	-50.6 ± 1.5
c (cell) (μM)^f	121	−	5.8	4.3	6.3	4.5	5.7	4.0
c (syr.) (μM)^f	789	−	61	100	61	100	61	100
k_d (10^{-3} s^{-1})^g	1800 ± 400	1400 ± 300	25 ± 4	3 ± 0.5	0.34 ± 0.01	$\sim$0.05	20 ± 4	0.55 ± 0.1
k_a (10^5 M^{-1} s^{-1})^h	1.4 ± 0.4	2.7 ± 0.7	1.5 ± 0.4	3.1 ± 0.8	1.6 ± 0.4	3.5 ± 1	2.7 ± 0.8	4.6 ± 1.4
K_D (nM)^i	$(13 \pm 5) \times 10^3$	$(5 \pm 2) \times 10^3$	68 ± 20	10 ± 3	2.1 ± 0.8	0.14 ± 0.05	37 ± 10	1.2 ± 0.4
$\Delta G°$ (kcal/mol)^j	-6.5 ± 0.2	-7.1 ± 0.2	-9.5 ± 0.2	-10.7 ± 0.3	-11.6 ± 0.3	-13.1 ± 0.3	-9.9 ± 0.2	-11.9 ± 0.3
$\Delta S°$ (cal/mol/K)^k	-24 ± 2	-22 ± 1	-52 ± 2	-58 ± 2	-79 ± 3	-95 ± 3	-93 ± 3	-130 ± 4

a Theoretical multivalency (*m*) and redundancy (*r*) of the interaction pairs (1:1 stoichiometry). *b* Labeling degree Γ estimated from analytical SEC. *c* Number of chelator heads per oligohistidine-tagged protein. *d* Equilibrium dissociation constant K_D determined by ITC. *e* Binding enthalpy $\Delta H°$ for a 1:1 interaction. *f* Concentrations in the cell (chelator head) and in the syringe (oligohistidine-tagged protein). *g* Dissociation rate constant k_d determined by time-resolved fluorescence measurements. *h* Association rate constant k_a determined by time-resolved fluorescence measurements. *i* Equilibrium dissociation constant K_D determined from k_a and k_d. *j* $\Delta G°$ determined from K_D obtained from kinetic data. *k* $\Delta S°$ determined from $\Delta G°$ (kinetic data) and $\Delta H°$ (ITC data).

were fitted by a model for irreversible second-order association kinetics:

$$S(t) = S_0 \cdot \frac{k_a(t - t_0) \cdot c^2}{1 + k_a(t - t_0) \cdot c} \qquad (2)$$

where k_a is the association rate constant, and c is the concentration of the reactants. The association kinetics were measured for the mono-NTA/oligohistidine tag interaction as described for the MCH. For measuring dissociation kinetics, a pre-equilibrated, stoichiometric mixture of mono-NTA (5 μM) and the oligohistidine tags (5 μM) was diluted 11 times. These curves were evaluated by fitting the differential equation for a reversible second-order reaction:

$$\frac{dS(t)}{dt} = k_a[S_0 - S(t)]^2 - k_d[S(t)] \qquad (3)$$

Details of the fitting procedure are described in Supporting Information.

The equilibrium dissociation constant K_D was determined from the rate constants:

$$K_D = k_d/k_a \qquad (4)$$

The standard free energies $\Delta G°$ with respect to 1 M concentration were calculated from the equilibrium dissociation constant K_D according to eq 5:

$$\Delta G° = RT \ln(K_D/1\ \text{M}) \qquad (5)$$

and the interaction entropies were determined from these $\Delta G°$ and the $\Delta H°$ values from ITC measurements based on eq 6:

$$\Delta G° = \Delta H° - T\Delta S° \qquad (6)$$

Results and Discussion

Grafting Metal-Chelating Moieties onto Branched and Cyclic Scaffolds. The MCHs were built up using *tert*-butyl-protected NTA synthons (**3**, **12**), which were grafted onto different scaffolds. The modular synthesis enabled versatile use of different scaffolds and is in principle also compatible with solid-phase synthesis. MCHs with two, three, and four NTA moieties were obtained, which were called bis-NTA (**17**), tris-NTA (**19**), and tetrakis-NTA (**18**), respectively. These MCHs are based on different types of scaffolds: while bis-NTA and tetrakis-NTA are based on a dendritic architecture with rather high conformational flexibility, tris-NTA is conformationally

relatively constrained due to the shorter chain length of synthon **12** compared to that of **3** and the cyclic scaffold. For probing the interaction with oligohistidine tags, carboxyfluorescein was coupled to the primary amino group of the chelator heads as a versatile and sensitive fluorescence reporter. The removal of excess nickel(II) ions after quantitatively loading the NTA groups without affecting the chelated metal ions was a critical issue, which was resolved by anion exchange chromatography at neutral pH. The attached carboxyfluorescein was beneficial for purification of the chelator heads after loading with metal ions and for determining the chelator concentrations photo-metrically. All measurements were carried out with the Ni(II) ion loaded fluorescein conjugates (Figure 1), which will nonetheless be referred to by their chelator heads (mono-NTA, bis-NTA, tris-NTA, and tetrakis-NTA).

To exploit the maximum conformational space of a hexa- and a decapeptide, we chose cumulated H6 and H10 tags for testing the chelator heads. The chelator heads presented 1−4 metal ions per molecule, leading to 2−8 possible coordinative bonds. On the other hand, H6 and H10 had the overall potential of 6 and 10 coordinations, respectively. The number of possible coordinative bonds (termed multivalency in the following) varied between the different chelator head/oligohistidine pairs. Thus, theoretically the number of histidines on the tag either over- or under-fulfill the coordination demands of the chelators in most instances with a single exception of tris-NTA hexahistidine interaction. This adds a new feature to the interaction, which we refer to as redundancy in the following. The theoretical multivalencies and redundancies in terms of possible coordination bonds are listed in Table 1 for every given interaction pair. The targets carrying the oligohistidine tags were two different monomeric proteins and one fluorophore, all linked to the N-terminus of the tag: (i) the ifnar2-EC, (ii) MBP, and (iii) carboxyfluorescein attached through an aminohexanoic acid linker.

Stable and Stoichimetrically Defined MCH/Oligohistidine Complexes. Binding of the Ni^{2+}-loaded chelator/fluorescein conjugates to H6- and H10-tagged ifnar2-EC (ifnar2-H6 and ifnar2-H10, respectively) was investigated by analytical SEC. The protein was equilibrated with a 1.5-fold stoichiometric excess of the chelator head, and mixture was separated by SEC.
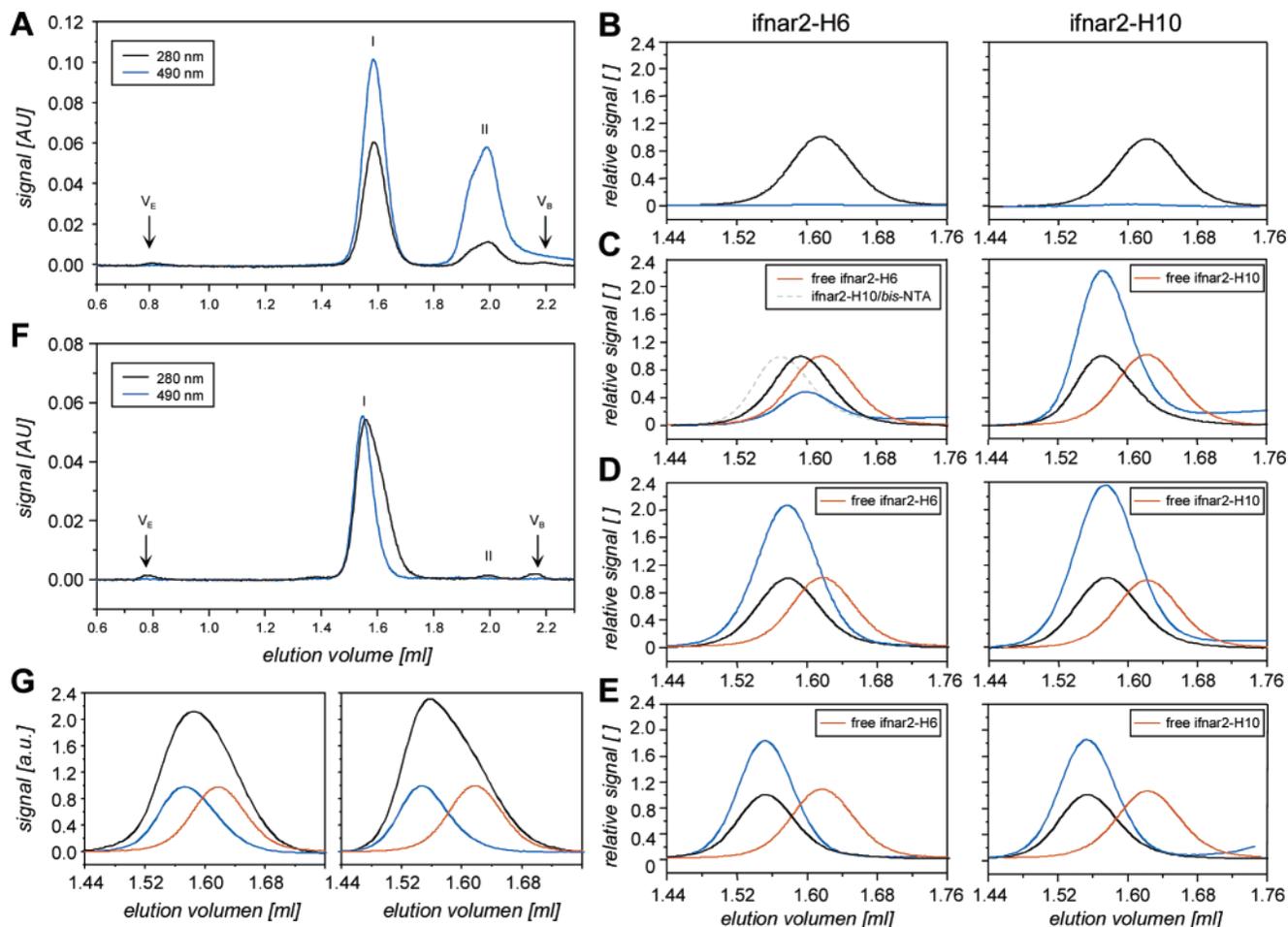
Figure 3. Stability and stoichiometry of chelator/oligohistidine complexes studied by analytical SEC. The absorbance was monitored at 280 nm (black) and 490 nm (blue) to discriminate the chelator/fluorescein conjugate and the protein. (A−E) ∼1.5-fold molar excess of the chelator/fluorescein conjugates. (A) Full chromatogram for tris-NTA/ifnar2-H6 showing the exclusion volume (V_E), the bed volume (V_B), the protein peak (*I*), and the peak of the chelator/fluorophor conjugate (*II*). (B−E) Comparison of the complexes with ifnar2-H6 (left panel) and ifnar2-H10 (right panel). (B) mono-NTA. (C) bis-NTA. (D) tris-NTA. (E) tetrakis-NTA. In C−E, the elution profile of the free protein is shown for comparison (orange). In the left panel of C, the protein peak of the right panel is shown (− − −). (F,G) SEC with ∼2-fold molar excess of the protein. (F) Full chromatogram for tetrakis-NTA with a stoichiometric excess of ifnar2-H6. (G) Protein peaks for bis-NTA/ifnar2-H10 (left panel) and tetrakis-NTA/ifnar2-H6 (right panel) complexes in comparison to the peak for ifnar2-EC alone (orange). For visual comparison, the peaks are shown in arbitrary units (a.u.).

A typical chromatogram with simultaneous detection at 280 and 490 nm is shown in Figure 3A, clearly showing one peak for the protein/chelator complex and one for the free dye eluting with the bed volume.

The relative absorbance signals at these two wavelengths within the protein peak, as well as the peak position, were used to estimate the amount of fluorescence dye attached to the protein. Shown in Figure 3B−E are the elution peaks of ifnar2-H6 and ifnar2-H10 with the different chelator heads measured under the same conditions. When ifnar2-H6 was incubated with mono-NTA, retention of the chelator head with the protein peak was hardly detectable (Figure 3B). A similar observation was made with ifnar2-H10 as well, but a slight increase of the labeling degree was observed. In contrast, when ifnar2-H6 was incubated with bis-NTA, the labeling efficiency substantially increased (Figure 3C), but the chelator head-to-protein ratio was still only 10−15%. At the same time, a minor shift of the chelator head peak relative to that of the protein peak was observed, suggesting dissociation of the complex during the SEC experiment. Interestingly, when ifnar2-H10 was incubated with bis-NTA, nearly 10-fold increase in labeling efficiency in

comparison of ifnar2-H6 was seen. Unlike ifnar2-H6, the chelator head and the protein peaks overlapped perfectly, suggesting that the bis-NTA/ifnar2-H10 complex remained stable during SEC. The increase in labeling efficiency was accompanied by a nearly quantitative shift of the protein peak toward higher apparent molecular weight, confirming a labeling efficiency of >90% for this interaction pair. Given four coordination sites on bis-NTA, both H6 and H10 over-satisfy the coordination demands, although by different redundancy factors. Thus, higher redundancy of the H10 tag significantly increased binding affinity toward this MCH.

When ifnar2-H6 was incubated with tris- and tetrakis-NTA, high labeling efficiencies (>90%) were observed, and the protein and the chelator head peaks perfectly coincided (Figure 3D,E). A shift of the protein peak was observed for tris-NTA, which was similar to the shift observed for the bis-NTA/ifnar2-H10 complex. For tetrakis-NTA, an even stronger shift of the complexed protein was observed (Figure 3E). No free protein was detectable, confirming labeling efficiencies close to 100% for these interaction pairs. These observations impressively confirmed the expected effect of increasing complex stability
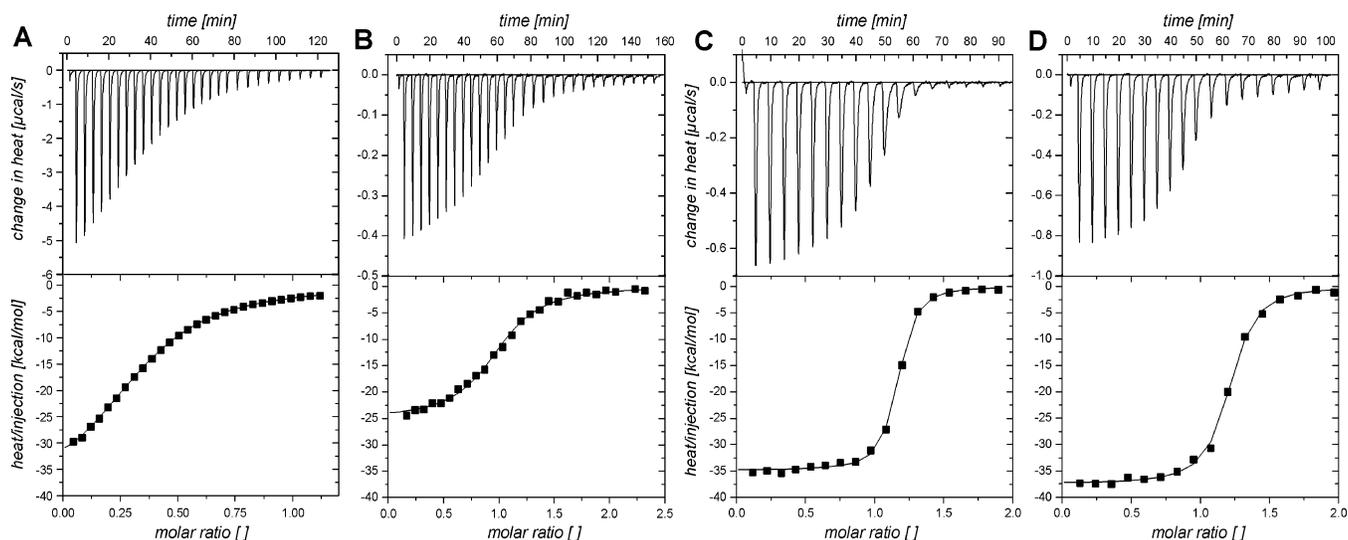
Figure 4. ITC thermograms (top) and titration curves (bottom) of the chelators titrated with MBP-H6. (A) mono-NTA. (B) bis-NTA. (C) tris-NTA. (D) tetrakis-NTA. The line corresponds to a fit of a standard interaction model assuming a single type of binding sites.

with increasing number of NTA groups (multivalency). Very similar chromatograms were obtained for the interaction of tetrakis-NTA and tris-NTA with ifnar-H10. The dye-to-protein ratio of the SEC chromatogram at stoichiometric excess of MCH already suggested a 1:1 stoichiometry of the complex. Stable and stoichiometric complex formation was further corroborated by SEC experiments with substoichiometric amounts of the MCH (Figure 3F,G). No free MCH was detectable under these conditions (Figure 3F). The protein peak was broadened as detected at 280 nm; strikingly, however, the peak observed at 490 nm was still eluting with the same shape and at the same elution volume as observed for stoichiometric excess of MCH (Figure 3G). Thus, a stable 1:1 interaction was confirmed for bis-NTA/H10, as well as for tris-NTA and tetrakis-NTA with both H6 and H10.

Similar labeling efficiencies were obtained with MBP-H6 and MBP-H10 as with ifnar2-H6 and ifnar2-H10 (data not shown), substantiating generic recognition of oligohistidine-tagged proteins by the MCH. The interaction was entirely specific for oligohistidine tags: when tagless ifnar2-EC or MBP was incubated with tris-NTA, no dye was detectable within the protein peak (data not shown). The interaction was fully reversible, as no complex was detectable after addition of 50 mM EDTA (data not shown).

Large Gains in $\Delta H°$ with Increasing Multivalency. ITC was performed to quantitatively assess and segregate the contributions of enthalpy and entropy toward the affinity constants for the chelator head binding to the oligohistidine tags. To understand the additive effects of increasing number of coordinations arising from the multivalent nature of the binding partners, the chelator heads were titrated with H6- and H10-tagged proteins and peptides. Typical titrations for all the chelator heads with MBP-H6 are compared in Figure 4. The complex formation was always net exothermic as would be expected for a reaction in which the coordination bonds are formed, but very different curvatures of the titration curves were observed depending upon the chelator head. To achieve sufficient curvature in the binding isotherm, titrations with mono-NTA were carried out at concentrations substantially higher than the concentrations used with the MCH. Figure 4A shows the

titration for mono-NTA (121 μM) with MBP-H6 (790 μM). While at these high concentrations the thermograms showed very large changes in heat, the curvature of the binding isotherm implies low affinity. Table 1 summarizes the enthalpy $\Delta H°$, interaction stoichiometry n, and equilibrium dissociation constant K_D, as obtained by fitting to the binding isotherm a 1:n interaction model, which assumes a single type of binding sites. Strikingly, a stoichiometric ratio of three mono-NTA units per MBP-H6 was observed, suggesting that all six histidines were coordinated under these conditions. A total $\Delta H°$ of 40.9 kcal/mol was obtained, implying that the average heat of coordination per mono-NTA was 13.6 kcal/mol.

This titration yielded a K_D of 14 ± 4 μM, which is in good agreement to what has been previously measured for mono-NTA/MBP-H6 interaction in solution.[35,36,38] The MCHs were titrated at much lower concentrations, and the clear sigmoidal shape of the binding isotherms corroborated affinities substantially higher compared to that of mono-NTA. Figure 4B shows the binding isotherm when bis-NTA (5.8 μM) was titrated with MBP-H6 (60.7 μM). The interaction parameters are listed in Table 1. A clear 1:1 stoichiometry was observed at the employed concentration, with a K_D of 270 nM. Thus, a 50-fold increase in affinity compared to mono-NTA was achieved. The $\Delta H°$ of 25 kcal/mol is nearly twice as much as that obtained for mono-NTA. When tris-NTA and tetrakis-NTA were titrated with MBP-H6, under conditions similar to bis-NTA, an even narrower transition of the binding isotherm was observed, indicating a further increase in affinity (Figure 4C,D). The stoichiometries were 1:1, and the K_D values determined for tris-NTA and tetrakis-NTA were 23 and 41 nM, respectively. Compared to that of bis-NTA, a substantial increment in $\Delta H°$ was observed for tris-NTA. However, compared to that of tris-NTA, no further increase in $\Delta H°$ was seen for tetrakis-NTA. This is in line with the fact that MBP-H6 allows formation of a maximum of six coordinative bonds for both tris-NTA and tetrakis-NTA.

Additive $\Delta H°$ at High Redundancies. All three MCHs were also titrated with MBP-H10, and similar titration curves (not shown) were obtained as for MBP-H6. These data are summarized in Table 1. In all the cases, 1:1 interactions were concluded from the fits. For a given MCH, a systematic increase
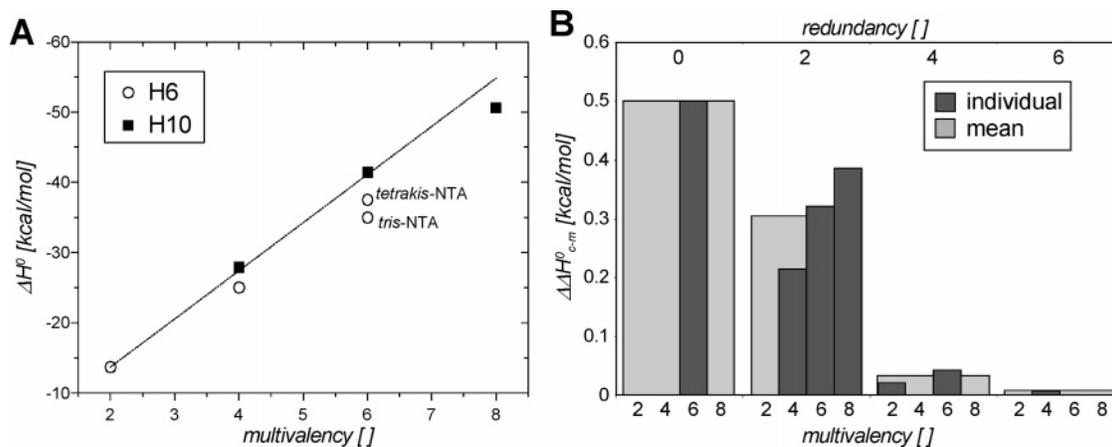
Figure 5. $\Delta H°$ of the chelator/oligohistidine pairs as obtained by ITC. (A) Correlation of the molar binding enthalpies $\Delta H°$ obtained for MBP-H6 ($\circ$) and MBP-H10 ($\blacksquare$) with the number of potential coordination bonds (multivalency). (B) Difference $\Delta\Delta H_{c-m}°$ between the measured and the theoretical, additive $\Delta H°$ for different multivalencies separated into different redundancies. The average $\Delta\Delta H_{c-m}°$ values for different redundancies are shown as gray bars in the background.

in $\Delta H°$ was observed for MBP-H10 compared to that of MBP-H6. Moreover, this difference ($\Delta\Delta H_{H10-H6}°$) increased with increasing multivalency. The K_D values for MBP-H10 with a given MCH, however, did not substantially differ as compared to those for MBP-H6 and even appeared to be systematically higher than those for the corresponding MCH/H6 complexes. This was surprising, as SEC conclusively indicated substantially increased affinity for MBP-H10 as compared to that for MBP-H6, at least for bis-NTA. Therefore, the binding affinities were independently determined by measuring the interaction kinetics (see below).

Figure 5A shows the $\Delta H°$ for all MCH/oligohistidine complexes as a function of theoretical number of coordination bonds.

Assuming a $\Delta H°$ of 13.6 kcal/mol (the $\Delta H°$ for the mono-NTA/MBP-H6 interaction) as the $\Delta H°$ for an NTA moiety coordinated by two histidines, the straight line represents the additive increase in heat as a function of number of coordinative bonds, which coincides well overall with the experimental data. The highest deviation from the theoretically expected $\Delta H°$ was observed for tris-NTA/H6, in agreement with the lowest redundancy of this interaction pair. The theoretical values for $\Delta H°$ were reached for bis-NTA/H10 and nearly reached for tris-NTA/H10. The difference $\Delta\Delta H_{c-m}°$ between measured $\Delta H°$ and calculated $\Delta H°$ is compared in Figure 5B for different multivalencies as a function of redundancy. This comparison reveals two striking features of multivalency and redundancy on $\Delta H°$: (i) the theoretical $\Delta H°$ values are generally reached closer with increasing redundancy. For redundancies of 4 and higher, the $\Delta\Delta H_{c-m}°$ were negligible. (ii) For pairs with the same redundancy, the $\Delta\Delta H_{c-m}°$ increased with increasing multivalency. Both effects can be ascribed to steric constraints upon complex formation:[46] high redundancy increases the possibility to adopt a complex, in which all coordination sites are occupied by histidines at a minimum strain; high multivalency increases the number of constraints, which have to be fulfilled to occupy all coordination sites simultaneously.

Increase in Complex Stability by Several Orders of Magnitude. To assess affinities and stabilities of the chelator/

oligohistidine complexes in a quantitative manner, association and dissociation kinetics were determined. All rate constants and equilibrium constants obtained from these experiments are summarized in Table 1. The change of fluorescence with time when mono-NTA (5 μM) was mixed with a carboxyfluorescein-labeled H6 peptide (5 μM) in a stopped flow setup is shown in Figure 6A. For analyzing the dissociation kinetics, the equilibrated complex (5 μM of each) was diluted 11-fold, and the emission was followed in real time (Figure 6B). The second-order kinetics for a 1:1 interaction (eq 3) with the appropriate initial conditions was iteratively fitted to the mixing and the dilution phases until the association and the dissociation rate constants converged. For the mono-NTA interaction with H6, a k_d of 1.8 s^{-1} and a k_a of 1.4×10^5 M^{-1} s^{-1} were determined. Using eq 4, we calculated a K_D value of 13 μM from these rate constants, which is in good agreement to the K_d obtained by ITC. Likewise, the kinetic constants were determined for H10. The mixing and the dilution phases are shown in Figure 6C,D. In comparison to H6, an approximately 2-fold higher k_a and a slight reduction in k_d were observed. The determined k_d and k_a were 1.4 s^{-1} and 2.7×10^5 M^{-1} s^{-1}, respectively, yielding a K_D of 5 μM. Thus, only a minor increase in affinity from H6 to H10 was observed, which contradicts the considerable differences observed in complex stability between H6 and H10 tags with immobilized chelators.[42]

For the MCH/oligohistidine complexes, no significant dissociation was observed upon dilution, which is in line with the substantially higher stability of these complexes observed in SEC. Therefore, the dissociation rate constants were determined by adding a 10-fold molar excess (5 μM) of MBP-H10 to an equilibrated complex of the chelator head and the labeled peptide (500 nM of each). Typical dissociation phases after correction and normalization are shown in Figure 7A. First-order kinetics was assumed under these conditions, and the dissociation rate constants were determined by fitting eq 1. The dissociation rate constants for the different chelator head/oligohistidine pairs are compared in Figure 7B. A decrease in the k_d of more than 4 orders in magnitude was observed from mono-NTA/H10 to tris-NTA/H10. With increasing number of NTA moieties of the MCH, the relative difference in complex stability between H6 and H10 increased. The most surprising feature, however, was

(46) Mammen, M.; Choi, S. K.; Whitesides, G. M. *Angew. Chem., Int. Ed.* **1998**, *37*, 2755–2794.
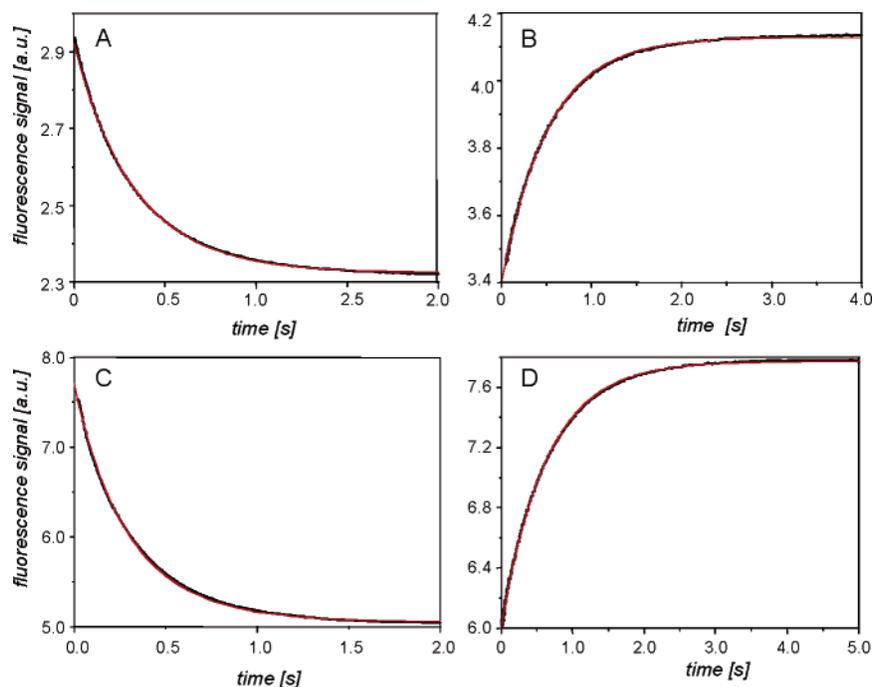
Figure 6. Kinetics of the interaction of mono-NTA with H6 (A,B) and H10 (C,D) as monitored by stopped-flow fluorescence. (A,C) Association kinetics. (B,D) Dissociation kinetics. The fit of the model is shown as a red curve.
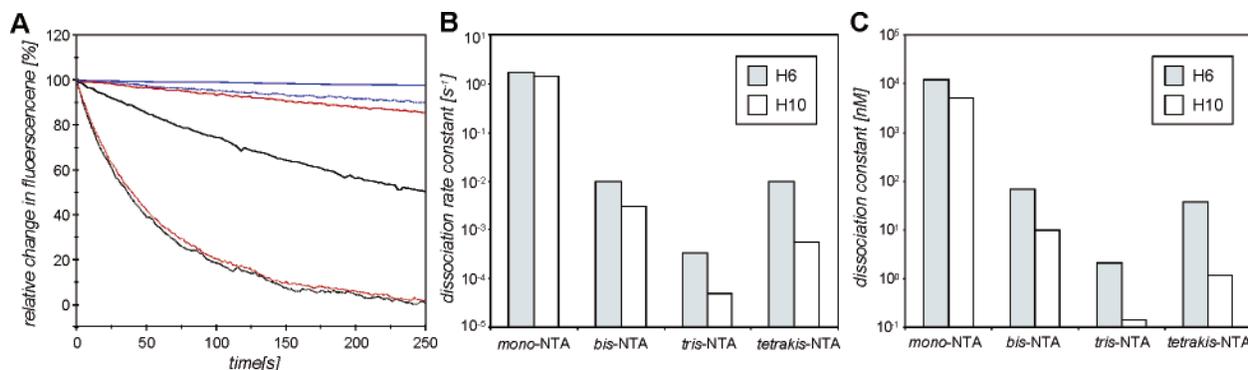

Figure 7. Dissociation kinetics of the MCH/oligohistidine complexes as characterized by fluorescence dequenching upon complex dissociation. (A) Dissociation kinetics for different MCHs in complex with H6 (···) and H10 (—) peptides as observed by fluorescence dequenching upon adding 10 μM unlabeled MBP-H10 (black: bis-NTA; blue: tris-NTA; red: tetrakis-NTA). The curves were processed as described in the Experimental Section. (B) Comparison of the k_d values for complexes of MCH with H6 (gray) and H10 (white) peptides obtained by a monoexponential fit of the dissociation curves as shown in B compared to the k_d obtained for mono-NTA. (C) Equilibrium dissociation constants as determined from the interaction kinetics in comparison for H6 (gray) and H10 (white).

the very low stability of the tetrakis-NTA/H6 complex, which dissociated nearly as fast as the bis-NTA/H6 complex. This is in marked contrast to SEC experiments, where the tetrakis-NTA/ifnar2-H6 complex showed substantially higher stability as compared to the bis-NTA/H6 complex. The association rate constants for the MCHs were determined by stopped-flow fluorescence as for mono-NTA. The association rate constants therefore were determined by fitting eq 2, as the contribution of complex dissociation to the curvature was negligible. The values are listed in Table 1.

The differences in the k_a for the different pairs were small overall. However, association of H10 was always faster than association of H6. This could be explained by a higher probability of a successful collision: the greater the number of histidines the higher the probability of encounter complex formation. This effect is not as pronounced for the increasing number of NTA moieties from mono- to tetrakis-NTA. Two

opposing factors might be at work: (i) association rate enhancement in proportion to the number of chelation sites and (ii) electrostatic repulsion resulting from the greater number of chelator heads carrying negative charges leading to more repulsion and hence a reduction in association rate.

High Loss in Entropy for Multivalent Complexes. We employed three different approaches for determining the stability and affinity of the chelator head oligohistidine tag interaction. The equilibrium dissociation constants (K_D) for all the chelator/oligohistidine pairs as calculated from the rate constants according to eq 4 are compared in Figure 7C. Table 1 summarizes the K_D obtained from ITC and the labeling efficiencies as estimated from SEC. Both ITC and kinetic measurements yielded very similar K_D values for mono-NTA/H6 and bis-NTA/H6 interaction. In contrast, the K_D values determined by ITC as compared to kinetic analysis were much higher for the bis-NTA/H10, tris-NTA/H6, tris-NTA/H10, and
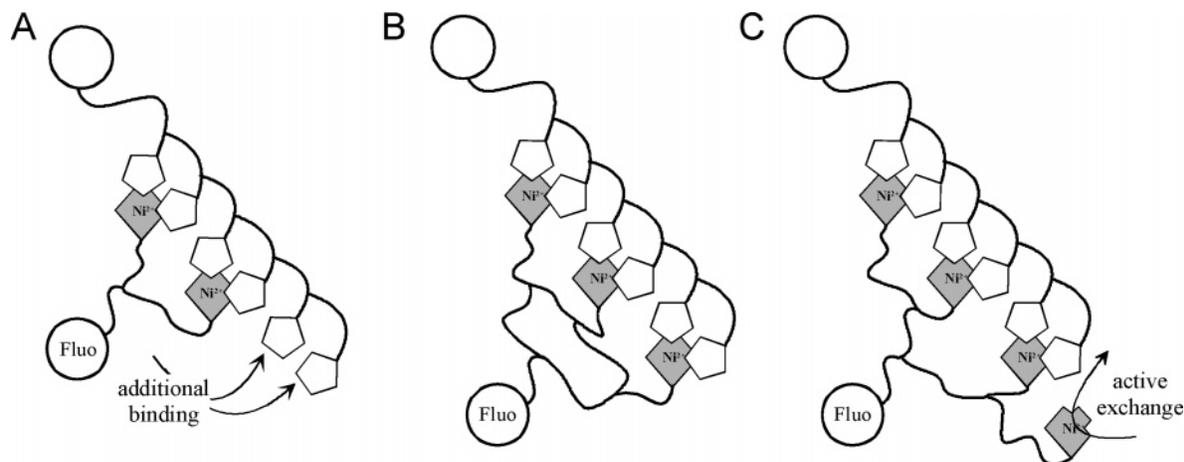
Figure 8. Schematic of different scenarios of multivalency and redundancy. (A) Redundancy of the oligohistidine tag (e.g., bis-NTA/H6) guarantees maximum $\Delta G°$, but allows nonstoichiometric complexes. (B) High multivalency and no redundancy as in the case of tris-NTA/H6 yields stable, stoichiometric complexes. (C) Redundancy of chelator groups as in the tetrakis-NTA/H6 complex provides docking sites for active exchange.
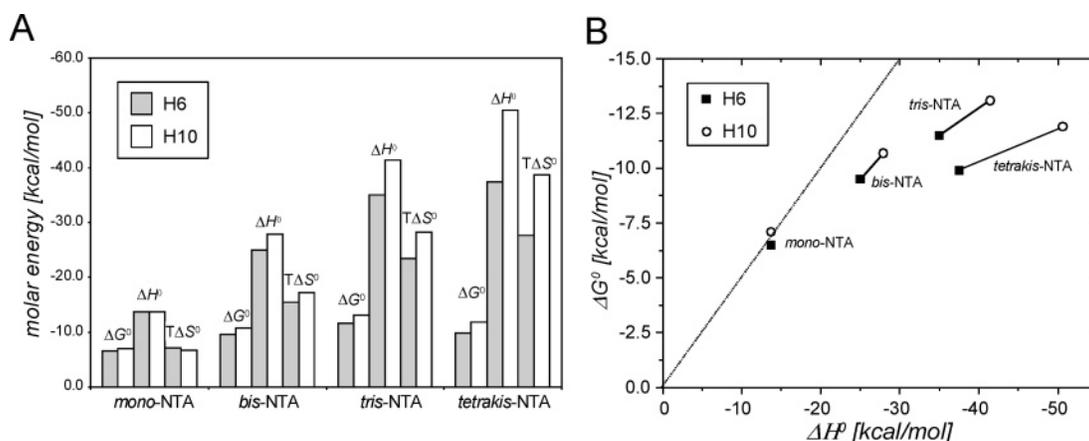

Figure 9. (A) Comparison of $\Delta H°$ and $\Delta G°$ and $T\Delta S°$ for all chelator complexes with H6 (gray) and H10 (white). (B) Correlation of $\Delta G°$ with $\Delta H°$ (i.e., effective multivalency) for the different chelator complexes with H6 (■) and with H10 (○). The points obtained for each MCH are linked by a line. The dotted line indicates additive $\Delta G°$ of a noncooperative multivalent interaction as defined by Whitesides and co-workers.[46]

tetrakis-NTA/H10 complexes. These discrepancies could arise from the experimental specifics related to the multivalent and redundant nature of the interaction partners:[47]

(i) The K_D values determined by ITC are orders of magnitude below the concentration applied in these measurements. Under these conditions, a titration curve contains only minute information about the affinity. At the same time, transient formation of the complexes with stoichiometries other than 1:1 due to a high concentration (micromolar) and high excess of the MCH in the cells cannot be completely ruled out (cf. Figure 8A), which may in turn slightly bias the binding isotherm. Therefore, extracting reliable affinity information from these measurements for the MCH is not feasible. However, in some instances the relative affinities can be conclusively determined (e.g., a significant increase in steepness of the binding isotherm for tetrakis-NTA/ H6 in comparison with that of bis-NTA/H6 clearly indicates a substantial decrease in K_D from bis-NTA/H6 to tetrakis-NTA/ H6 complex). This observation is also in good agreement with the labeling efficiencies as obtained from SEC experiment.

(ii) The stability of the tetrakis-NTA/H6 complex as determined by the competition assay contradicts the relatively higher stability and affinity compared to bis-NTA/H6 as is evident from

SEC and ITC measurements. We interpret this apparently low complex stability by invoking nonspontaneous dissociation: H6 bound to tetrakis-NTA was actively exchanged by the competing MBP-H10 due to the additional, noncomplexed NTA moiety, which can act as a docking site for a competitor (Figure 8C).

This would be an interesting mechanism based on redundancy, which could be exploited for applications that require fast exchange of the tag bound to the MCH by another tag. Since this effect is probably a specific feature of the tetrakis-NTA/H6 complex, the K_D values obtained from kinetic measurements appeared generally more reliable compared to the K_D obtained from ITC. Therefore, the free energies $\Delta G°$ of complex formation were determined from the K_D obtained from kinetic data using eq 5. These $\Delta G°$ values are shown in comparison to the $\Delta H°$ and the resulting $T\Delta S°$ for all the pairs in Figure 9A. In all the cases, $\Delta H°$ was substantially higher than $\Delta G°$ (i.e., the $\Delta S°$ was negative). For a given histidine tag, the $\Delta S°$ increased with increasing number of NTA moieties, indicating an increasing "penalty" with the number of coordination bonds being formed. This is not surprising for a multivalent interaction between two flexible binding partners, both of which substantially lose conformational freedom upon complex formation.

(47) Kitov, P. I.; Bundle, D. R. *J. Am. Chem. Soc.* **2003**, *125*, 16271−16284.

The correlations of ΔG° with multivalency and with ΔH° are shown in Figure 9B. The additive increase of ΔG° with multivalency of a noncooperative multivalent interaction (as defined by Whitesides and co-workers)[46,48] is indicated by a dotted line. For all MCH/oligohistidine pairs, substantially less than additive ΔG° was obtained, that is, negative cooperativity, which is typical for multivalent interactions.[46] The good correlation of ΔG° with ΔH° supports that complex formation is mostly driven by enthalpy even at high redundancies (Figure 9B): a constant increase was observed for mono-, bis-, and tris-NTA, which did not significantly differ for H6 and H10. This correlation did not hold true for the tetrakis-NTA/oligohistidine complexes, for which significantly lower $\Delta G^\circ/\Delta H^\circ$ ratios were obtained. The k_d values determined for tetrakis-NTA, however, were probably too high due to the active exchange mechanism as described above, which could account for the relative too low ΔG°. Since the structure of tetrakis-NTA is much more flexible compared to that of tris-NTA, a larger loss in entropy upon complex formation could also be the reason for a lower gain in ΔG°. However, not only flexibility of linkers[49] but also the different topologies have been shown to play a key role for optimizing the free energy of multivalent complexes.[47] For this reason, substantial differences in ΔS° are expected for the branched MCH bis-NTA and tetrakis-NTA, compared to that of the cyclic tris-NTA.

Conclusions

We have designed high-affinity recognition units for short peptides by exploiting multivalent coordinative interaction with the oligohistidine tag. A tremendous increase spanning 4 orders of magnitude in affinity and complex stability was obtained for the MCH compared to that of the conventional mono-NTA. At the same time, fast reversibility of the interaction (switchability) under mild conditions (imidazole, EDTA) was maintained, which is an exceptional advantage of multivalent interactions.[15] A prominent characteristic of most of the MCH/oligohistidine complexes at 1:1 stoichiometry was an excess of coordination sites either on the tag, or, in one case, on the chelator head. Because of the already relatively high affinity of an individual dihistidine/Ni:NTA interaction ($\sim$10 μM), this feature, which we called redundancy, has some important consequences. First, complex stoichiometries should depend on the absolute concentrations: while clear 1:1 stoichiometries were observed at low concentrations ($<$1 μM), other complex stoichiometries cannot be excluded at high concentrations or at substantial relative shortage in amount of the redundant partner. This feature hampered precise assessment of equilibrium binding constants by ITC, but opened new possibilities for actively exchanging one ligand by another by docking the competitor through an excessive binding site. Second, a substantial redundancy of histidines was required to reach the theoretical, additive ΔH°, indicating that steric constraints interfered with full coordination. This observation suggests that the MCHs do not bind a contiguous stretch of histidines in case of redundant tags. Owing to the degenerate interaction motif, however, the structures of the complexes are probably not well defined because individual histidines within the histidine tag can exchange coordination positions, in particular in complexes with high redundancies. Comparison of ΔG° and ΔH° of complex formation revealed an increasing loss of entropy with increasing multivalency (i.e., declining gain in ΔG° relative to ΔH°). We ascribe this to the high flexibility of both interaction partners, leading to a dramatic loss of conformational freedom upon complex formation. Thus, further improvement of binding affinities would require more rigid scaffolds for the recognition unit. On the basis of these insights, improving the affinity and selectivity of the interaction with the MCH by tailoring *tags* with appropriately positioned histidines appears promising. Other than mere affinity enhancement, more ambitious differential binding could also be envisioned. This interaction gives a synthetic control over the design of the recognition unit and a recombinant combinatorial control over the tags.

These high-affinity, yet switchable chemical recognition units open a wide field of possible applications. In contrast to conventional approaches based on protein-based recognition,[8-11,14] both the MCH and the recognized oligohistidine peptide are small, resulting in a highly localized attachment to the protein. Spectroscopic probes of different nature can be coupled to the MCH in a chemically and structural defined manner as already demonstrated in this work. Other functional units such as lipids, poly(ethylene glycols), and other polymers or nanoparticles could be site-specifically coupled to proteins in a reversible manner. Also for immobilization on surfaces, multivalent chelators could provide distinct advantages.[42] At the same time, metal ions are incorporated into proteins, which could be used as additional probes. Since the oligohistidine tag is the most frequently applied affinity tag in heterologous protein expression, generic and widespread application of such conjugates is guaranteed.

Supporting Information Available: Detailed description of the synthesis, purification, and spectroscopic characterization of the compounds, and a description of the fitting procedure for reversible bimolecular interaction kinetics. This material is available free of charge via the Internet at http://pubs.acs.org.

JA050690C

(48) Jencks, W. P. *Proc. Natl. Acad. Sci. U.S.A.* **1981**, *78*, 4046–4050.
(49) Glick, G. D.; Toogood, P. L.; Wiley, D. C.; Skehel, J. J.; Knowles, J. R. *J. Biol. Chem.* **1991**, *266*, 23660–23669.